



Design, synthesis and evaluation of 2-amino-4-*m*-bromoanilino-6-arylmethyl-7-*H*-pyrrolo[2,3-*d*]pyrimidines as tyrosine kinase inhibitors and antiangiogenic agents¹

Alem Gangjee^{a,*}, Ying Zhao^a, Sudhir Raghavan^a, Michael A. Ihnat^b, Bryan C. Disch^b

^a Division of Medicinal Chemistry, Graduate School of Pharmaceutical Sciences, Duquesne University, Pittsburgh, PA 15282, United States

^b Department of Cell Biology, School of Medicine, University of Oklahoma Health Sciences Center, Oklahoma City, OK 73104, United States

ARTICLE INFO

Article history:

Received 26 March 2010
Revised 17 May 2010
Accepted 18 May 2010
Available online 25 May 2010

Keywords:

Multiple receptor
Tyrosine kinase inhibitors
Antiangiogenic agents

ABSTRACT

A series of 2-amino-4-*m*-bromoanilino-6-benzyl pyrrolo[2,3-*d*]pyrimidines analogues **4–12** were synthesized and evaluated as inhibitors of receptor tyrosine kinases (RTKs). These analogues were synthesized from the appropriate α -bromomethylbenzylketones via cyclocondensation with 2,6-diamino-4-pyrimidone to afford the 2-amino-4-oxo-6-substituted benzyl pyrrolo[2,3-*d*]pyrimidines. Chlorination at the 4-position followed by displacement with 3-bromoaniline or 3-bromo-*N*-methylaniline and methylation of the 7-NH afforded the target compounds. Remarkably, dimethylation of both the 4-N and N7 afford whole cell EGFR inhibitors that are more cytotoxic than clinically used erlotinib and mono-methylation at the 4-N or N7 affords more cytotoxic whole cell PDGFR- β inhibitors than clinically used sunitinib. Methylation at either the 4-N or N7 position was detrimental to whole cell VEGFR-2 inhibition. The inhibitory data against the RTKs in this study demonstrates that methylation of the 4-NH and/or the 7-NH influences both the specificity and potency of RTK inhibition.

© 2010 Elsevier Ltd. All rights reserved.

1. Introduction

Angiogenesis is the formation of new blood vessels from pre-existing vasculature. Based on Folkman's seminal observation, in order to grow beyond a few millimeters in diameter, solid tumors depend on the newly formed vasculature network around the tumor mass to provide nutrients and to remove metabolic waste.² It is now well established that angiogenesis plays a key role in the growth of solid tumors, tumor invasion and metastasis.^{3–5} The most pronounced factor that triggers angiogenesis is the activation of receptor tyrosine kinases (RTKs) which regulate the transduction of signals from the extracellular domain of endothelial cells to the nucleus.⁶ Abrogation of angiogenesis via RTK inhibition provides an approach for the treatment of cancer. Dysfunctional, hyperactive growth factor RTKs including platelet-derived growth factor receptor (PDGFR), fibroblast growth factor receptor (FGFR), vascular endothelial growth factor receptor (VEGFR), insulin-like growth factor receptor (IGFR) and epidermal growth factor receptor (EGFR)

among others have been associated with several tumors and play a role in tumor angiogenesis.⁷

Previously the majority of development of RTK inhibitors was focused on targeting single RTKs. Examples of such clinically used agents include gefitinib (Iressa, specific EGFR inhibitor; approved for use in the treatment of non-small lung cancer) and erlotinib (Tarceva, specific EGFR inhibitor; approved for the treatment of non-small lung cancer) (Fig. 1).^{8–10} Single RTK targeting is specific and does not allow for off target inhibition of other RTK and hence pose little toxicity issues. However, the tumors often survive through an alternative signaling pathway to afford angiogenesis and thus develop resistance to these specific RTK inhibitors. The current paradigm for RTK inhibitors in cancer chemotherapy is the inhibition of multiple, rather than single, RTKs. Recently, additional preclinical studies show that simultaneous inhibition of multiple kinases by single-agents has the potential to increase antitumor activities. The FDA has approved sunitinib and sorafenib (Fig. 1) as multi targeted agents which show clinical benefit as antitumor agents with minor side effects.^{11,12}

Using the information provided by the crystal structure of cyclic-AMP-dependent protein kinase, a general pharmacophore model of ATP and the ATP binding site of RTKs has been proposed¹³ and refined.¹⁴ We have used a general pharmacophore in the anticipation that such a general pharmacophore will afford multi-kinase inhibitory agents. The model proposed (Fig. 2) consists of an Adenine

Abbreviations: RTKs, receptor tyrosine kinases; PDGFR, platelet-derived growth factor receptor; FGFR, fibroblast growth factor receptor; IGFR, insulin growth factor receptor; VEGFR, vascular endothelial growth factor receptor; EGFR, epidermal growth factor receptor; CAM, chicken embryo chorioallantoic membrane.

* Corresponding author. Tel.: +1 412 396 6070; fax: +1 412 396 5593.

E-mail address: gangjee@duq.edu (A. Gangjee).

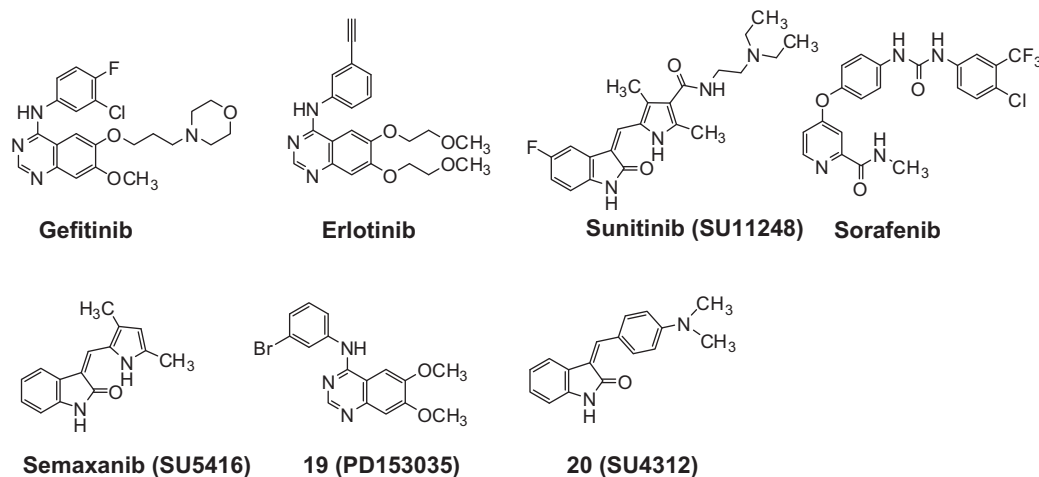


Figure 1. Structures of RTK inhibitors.

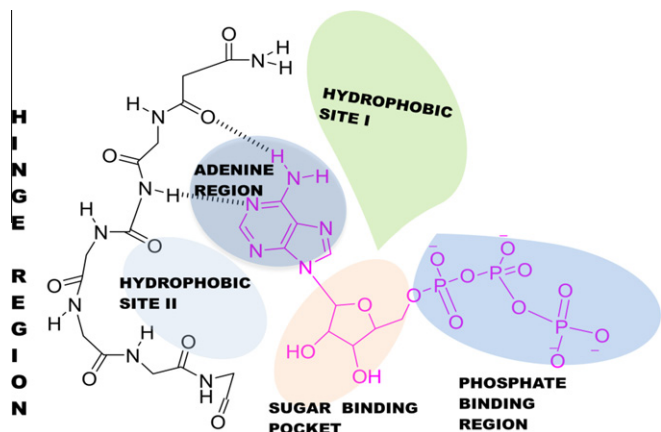


Figure 2. The general ATP-binding site of RTKs. Pharmacophore model of the ATP-binding site of protein kinases. ATP is in pink.

region which is a hydrophobic binding site for the adenine ring of ATP as well as for the heterocyclic scaffold of inhibitors such as quinazolines and pyrimidines. The N1- and N6-amino nitrogen of the adenine ring of ATP are hydrogen bonded to two amino acid residues of the Hinge region. The Sugar binding pocket in the ATP binding site accommodates the sugar moiety of ATP and the Phosphate binding region binds the triphosphate moiety of ATP. In addition, a Hydrophobic site I extends in the direction of the lone pair of the N7 of ATP and a Hydrophobic site II lies below the Adenine region. Neither hydrophobic site is used by ATP for binding.

On the basis of the general pharmacophore model, Gangjee et al.¹⁵ embarked on the design of RTK inhibitors using the pyrrolo[2,3-*d*]pyrimidine scaffold with an additional 2-NH₂ moiety which is not present in most other 6–6 or 6–5 ring system RTK inhibitors. The 2-NH₂ group in our compounds provides a third H-bonding moiety in the Hinge region of RTKs, and was anticipated to increase binding and consequently potency against RTKs. This has recently been shown to be true in most instances, but is dependent on the nature of the scaffold and its substitutions.^{16,17}

An initial series of 2-amino-4-*m*-bromoanilino-6-arylmethylpyrrolo[2,3-*d*]pyrimidines of structures shown in Figure 3 indicated that substitution on the 6-aryl moiety dictates both the selectivity and potency against a variety of RTKs. The most potent compounds of this series were 1–3 (Fig. 3).¹⁵

Compounds 1–3 were docked into the active site of the X-ray crystal structure of EGFR bound to erlotinib (PDB: 1M17¹⁸) using

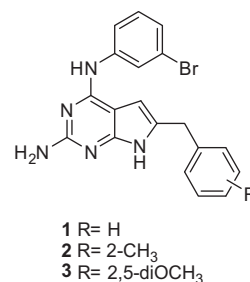


Figure 3. RTK inhibitors.¹⁵

Flexx 3.1.2.¹⁹ Clustering and analysis of the docked poses of the compounds indicated multiple low energy binding modes for the compounds consistent with the literature reports for docked and X-ray crystal structures of small molecules in kinases.²⁰ Of the different possible binding modes, three low energy, high scoring important binding modes for 1–3 are shown in Figure 4. In Mode I, the 2-NH₂ group, N3-nitrogen and 4-NH can hydrogen bond with the Hinge region; the 4-anilino group interacts with Hydrophobic site I and the 6-substituted benzyl ring interacts with the Sugar binding pocket. In binding Mode II hydrogen bonds with the Hinge region can be formed by the 2-NH₂ group, N3-nitrogen and 4-NH: the 4-anilino group interacts with hydrophobic site II and the 6-substituted benzyl ring interacts with the Sugar binding pocket. Binding Mode III is obtained from Mode I by rotating 180° around the C–N bond between C-2 and the 2-NH₂. In Mode III, the N7-pyrrolo nitrogen replaces the 4-NH and hydrogen bonds with the Hinge region. The anilino group interacts with the Sugar binding pocket and the 6-substituted benzyl ring interacts with the Hydrophobic site I (Fig. 4). These binding modes were among those observed within 2 kcal/mol of the lowest energy poses obtained during multiple docking iterations of 1–3 using Flexx 3.1.2.

We reasoned that hypothetical modes of binding illustrated in Figure 4 could be substantiated by introduction of strategically placed methyl substitutions at the N7- and/or 4-N positions and evaluation of the resulting analogues for RTK activity. These methyl substitutions would preclude the N7- and/or 4-N from functioning as a hydrogen bond donor as required by all three proposed modes of binding (Fig. 4). Thus, starting with the three most potent compounds (1–3) previously synthesized, each analogue was substituted in the 4-N position (compounds 4, 7, and 10), the N7-position (5, 8, and 11) and both the 4-N and N7-positions (6, 9, and 12) with methyl group(s) (Fig. 5). Thus, if Mode I and/

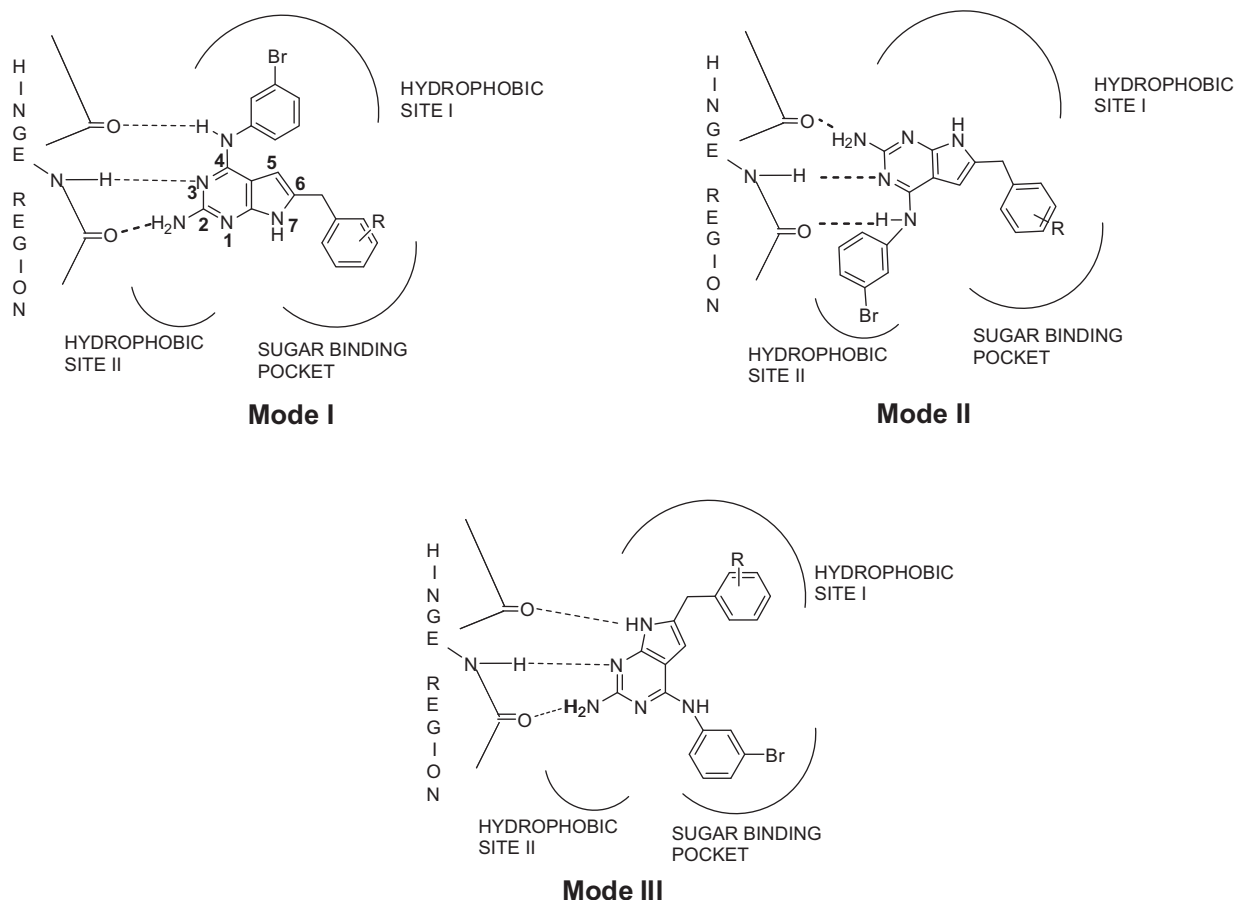


Figure 4. Proposed binding modes of pyrrolo[2,3-*d*]pyrimidines to RTKs.

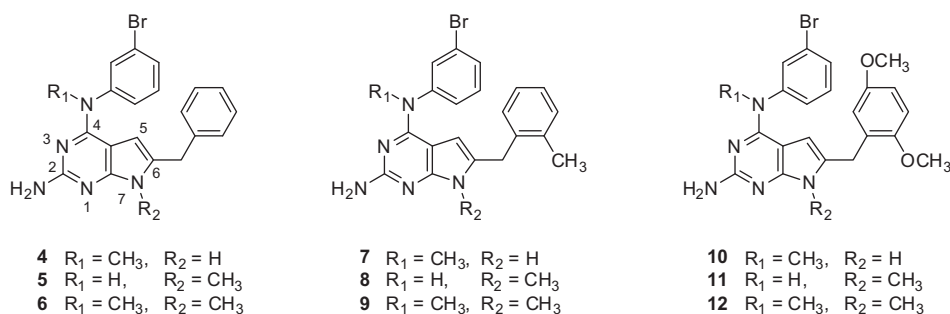


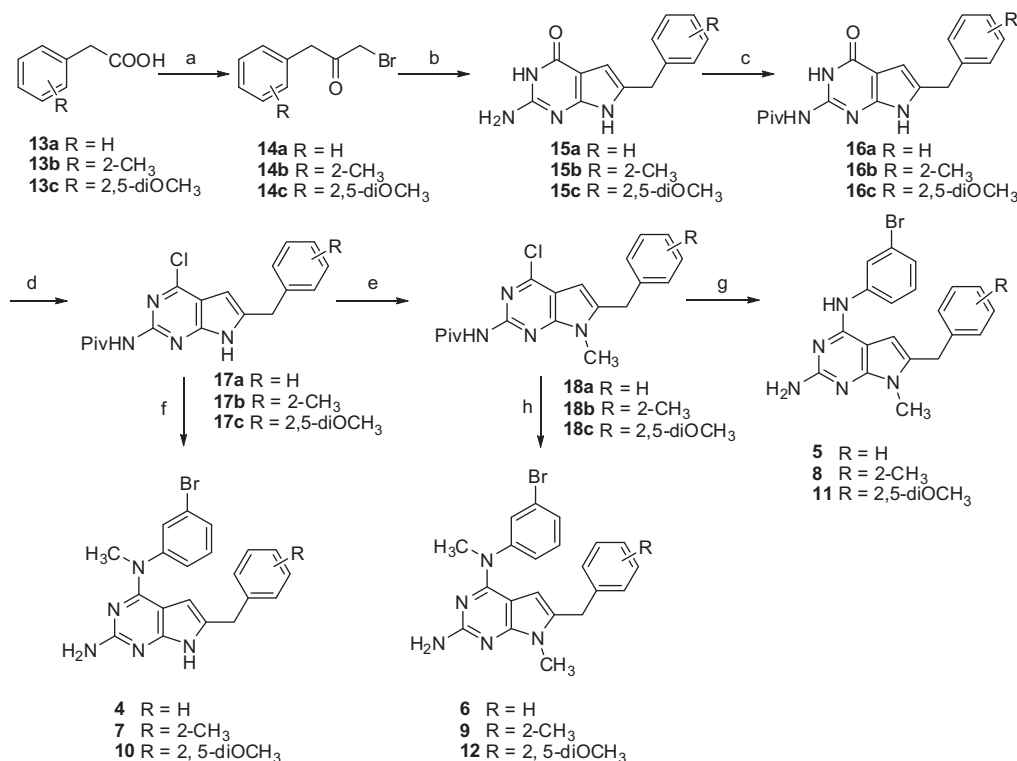
Figure 5.

or Mode II was/were the only binding mode(s) and the 4-NH was necessary for binding, compounds **4**, **6**, **7**, **9**, **10**, and **12** should be poorly active; on the other hand, if Mode III was the only binding mode and the N7-H was necessary for binding, compounds **5**, **6**, **8**, **9**, **11**, and **12** should be poorly active. If however, all three modes were possible, only compounds **6**, **9**, and **12** should be poorly active since they lack H-bonding donor ability at both the 4-N and N7. In addition, methylation at the N7- and/or the 4-N also influences the conformation of the 6-substituent and/or the 4-substituent (respectively) with respect to the pyrrolo[2,3-*d*]pyrimidine scaffold and could also, in part, influence the potency and selectivity of the methylated compounds compared with the unmethylated analogs.

2. Chemistry

The synthetic method for target compounds **4–12** is shown in Scheme 1. The key intermediates in the synthesis are 2-piv-

aloylamino-4-chloro-6-(substitutedbenzyl)-pyrrolo[2,3-*d*]pyrimidine, **17a–c**, which were converted to the target compounds via nucleophilic substitution with appropriate anilines or methylation with MeI followed by nucleophilic substitution with appropriate anilines. Compounds **17a–c** were synthesized from commercially available acids **13a–c**, respectively, via treatment with thionyl chloride followed by diazomethane (generated from *N*-nitroso-*N*-methyl urea) in an ice-bath to afford the α -diazoketones, which were converted to the α -bromoketones **14a–c** with 48% HBr solution. Cyclocondensation of **14a–c** with 2,6-diamino-4-hydroxypyrimidine at room temperature in DMF for 3 days afforded regioselectively the 2-amino-4-oxo-6-benzylpyrrolo[2,3-*d*]pyrimidines **15a–c** in 20–37% yield. Protecting the 2-amino group of **15a–c** with pivalic anhydride afforded **16a–c** in 20–37% yield, which were further converted to **17a–c** in 31–78% yield via chlorination with POCl₃. With the key intermediates **17a–c** in hand, the target compounds **4**, **7**, and **10** were obtained by nucleophilic



Scheme 1. Synthesis of **4–12**. Reagents and conditions: (a) (1) SOCl₂, benzene, reflux, 1 h; (2) CH₂N₂/Et₂O, 30 m; (3) 47.5% HBr, 70–80 °C, 1 h; (b) 2,6-diamino-4-hydroxypyrimidine, DMF, rt, 3 days; (c) Piv₂O, reflux, 3 h; (d) POCl₃, reflux, 3 h; (e) MeI, NaH, THF, 0–25 °C; (f) (1) *i*-PrOH, 3-bromo-*N*-methyl aniline, 2–3 drops of concd HCl, reflux, 30 m; (2) 15% KOH, 1,4-dioxane, reflux, 10 h; (g) (1) *i*-PrOH, 3-bromoaniline 2–3 drops of concd HCl, reflux, 30 m; (2) 15% KOH, 1,4-dioxane, reflux, 10 h; (h) (1) *i*-PrOH, 3-bromo-*N*-methyl aniline, 2–3 drops of concd HCl, reflux, 30 m; (2) 15% KOH, 1,4-dioxane, reflux, 10 h.

displacement of the 4-chloro moiety of **17a–c** with 3-bromo-*N*-methyl aniline in isopropyl alcohol at reflux for 4 h in the presence of 2–3 drops of concd HCl and then deprotected with 15% potassium hydroxide in 14–20% yield. Methylation of **17a–c** with MeI at 0–5 °C in THF gave **18a–c** in 57–77% yield, which afforded the target compounds **5**, **8**, and **11** in 42–58% yield via nucleophilic substitution with 3-bromoaniline followed by deprotection of the 2-pivaloyl group. The target compounds **6**, **9**, and **12** were obtained in 27–33% yield by displacement of the 4-chloro moiety of **18a–c** with 3-bromo-*N*-methyl aniline and deprotection of the 2-pivaloyl group.

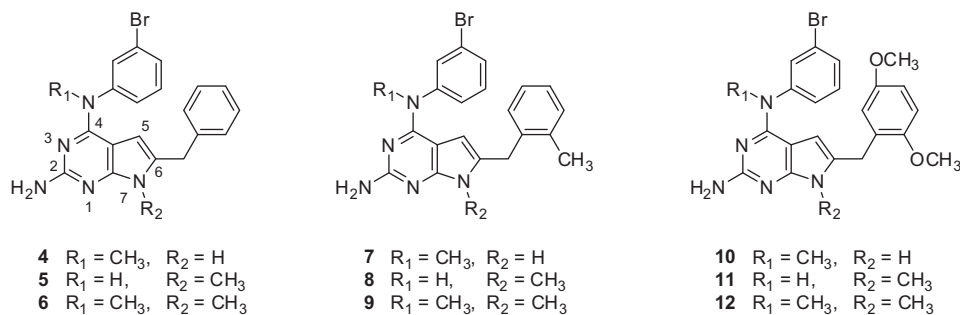
3. Results and discussion

The RTK inhibitory activity of the compounds were determined using human tumor cells known to express high levels of EGFR, VEGFR-2, and PDGFR- β , respectively, as we have reported previously and are listed in Table 1.¹⁵ Cytotoxicity studies against the growth of A431 cells, which over-express EGFR, in culture, were also carried out for these compounds and are listed in Table 1. In all cases, assays were carried out 2–3 times with 4–5 replicates per assay. In addition, the effect of **4–12** on new blood vessel formation (angiogenesis) was assessed using the chicken embryo chorioallantoic membrane (CAM) assay, a standard test for angiogenesis and are listed in Table 1. Since the IC₅₀ values of compounds vary under different assay conditions (e.g., ATP concentrations etc.) we used standard (control) compounds in each of the evaluations. Clinically used erlotinib and *N*-(3-bromophenyl)-6,7-dimethoxyquinazolin-4-amine **19** (PD153035, Fig. 1)²¹ were used as standards for EGFR inhibition. Clinically used sunitinib and (Z)-3-[4-(dimethylamino)benzylidene]indolin-2-one, **20** (SU4312, Fig. 1)²² were used as standards for PDGFR- β inhibition. Sunitinib and semaxanib (Fig. 1) were used as standards for VEGFR-2 inhibi-

tion and semaxanib was used as a standard for the CAM assay and cisplatin was used as a standard for the A431 cytotoxicity assay.

In the EGFR whole cell assay (Table 1), mono-methylation on either the 4-NH or N7-position resulted in decreased activity or inactive compounds compared with the standard, **19** but more cytotoxic (**12**) or equipotent with erlotinib. The 4-N, N7-dimethylated compounds **9** and **12** were the most potent and were eight-fold and 25-fold more potent than the lead compounds **2** and **3**, respectively. However, the 4-NH, N7-dimethylated compound **6** was much less potent than its lead compound **1** indicating that the substitution on the 6-benzyl ring is also an important determinant for activity. Compounds **1** and **9** were as active as erlotinib, an EGFR inhibitor, while **12** was twice as active against EGFR as compared to erlotinib.

In an attempt to explain the activity against EGFR in the whole cell assay, molecular modeling studies were performed for **1–12** using Flexx 3.1.2 using docking into the X-ray crystal structure of the 4-anilinoquinazoline inhibitor erlotinib in EGFR (PDB ID: 1M17). Multiple low energy binding modes were observed for all the docked compounds. The binding mode presented in Figure 6 for **1–3** was observed to be within 2 kcal/mol of the lowest energy pose and permitted comparison between the proposed binding modes of the three molecules. All the molecules form hydrogen bonds with the Hinge region using the 2-NH₂ moiety. Additional hydrogen bonding using the N3-nitrogen is observed for **1** and **2** but not **3**. Hinge region hydrogen bonds with the 4-NH is observed for **1** and **3** but not **2**. This explains, in part, the greater potency of **1** against EGFR compared with **2** and **3**. The anilino rings of the three compounds reside in Hydrophobic site II and are flanked by Leu694, Leu768, and Pro770. The 6-benzyl moieties of the molecules extend into the Sugar binding pocket and interact with a hydrophobic pocket formed by Leu694, Phe699, and Val702. The altered conformations of the side chain benzyl ring in **2** due to

Table 1IC₅₀ values (μM) of kinase inhibition, A431 cytotoxicity, and inhibition of the CAM assay

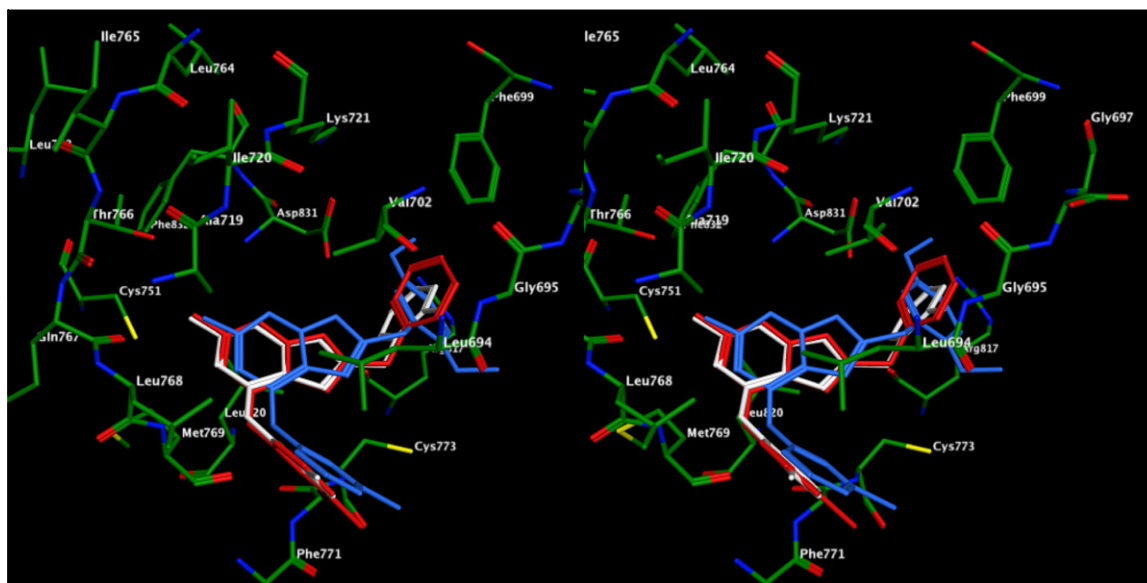
Compound	EGFR inhibition	VEGFR-2 inhibition	PDGFR-β inhibition	A431 Cytotoxicity	CAM angiogenesis inhibition
1	1.67	>50	>50	31.8	ND
2	9.19	0.25	>50	1.21	1.21
3	12.62	0.62	8.92	>50	1.32
4	53.1	89.2	>500	45.7	1.56
5	>200	>200	2.8	27.9	6.22
6	253.6	>200	71.7	50.9	2.6
7	31.2	>200	34.8	>500	0.93
8	12.8	116.3	>500	204.3	3.0
9	1.2	>200	>500	226.3	1.6
10	143.5	>200	1.3	197.4	0.83
11	>200	>200	348.0	35.6	3.3
12	0.5	>200	>500	94.1	2.05
19	0.23				
20			3.75		
Semaxanib		12.9			0.04
Cisplatin				10.6	18.2
Erlotinib	1.2	124.7	83.1		29.1
Sunitinib	172.1	18.9	12.2		1.3

the 2'-CH₃ and in **3** due to the 2',-5'-dimethoxy cause the benzyl ring to extend away from Val702, reducing the extent of hydrophobic stabilization of these molecules. Ligand interaction plots for **1–3** are shown in Figure 7(A–C).

Docked poses of the 4-N methylated compound **4** in EGFR (PDB ID: 1M17) show the loss of hydrogen bonding to the backbone of Met769 afforded by the 4-NH group in the unmethylated lead compound **1** (Figs. 8 and 9). Additionally, to accommodate the 4-N methyl group, **4** is oriented farther from the Hinge region as compared to **1**. This results in the loss of a hydrogen bond of the

N3-nitrogen with the backbone of Met769. Additional binding interactions afforded by other portions of **4** are analogous to those seen in **1**. This loss in H-bonding of the N3 in **4** could explain, in part, its reduction in whole cell activity against EGFR as compared to **1** which lacks the 4-N methyl group (see Figs. 8 and 9).

When comparing the 4-N, N7-dimethylated compounds **6**, **9**, and **12**, it was noted that the whole cell activity of the compounds increase with increasing size of the substitution on the 6-benzyl ring. This trend is in contrast to that for the lead compounds **1–3**. Docking studies with **12** (Figs. 10 and 11) indicated that this

**Figure 6.** Stereoview. Overlay of docked poses of **1** (red), **2** (white) and **3** (blue) in EGFR active site (PDB code 1M17).

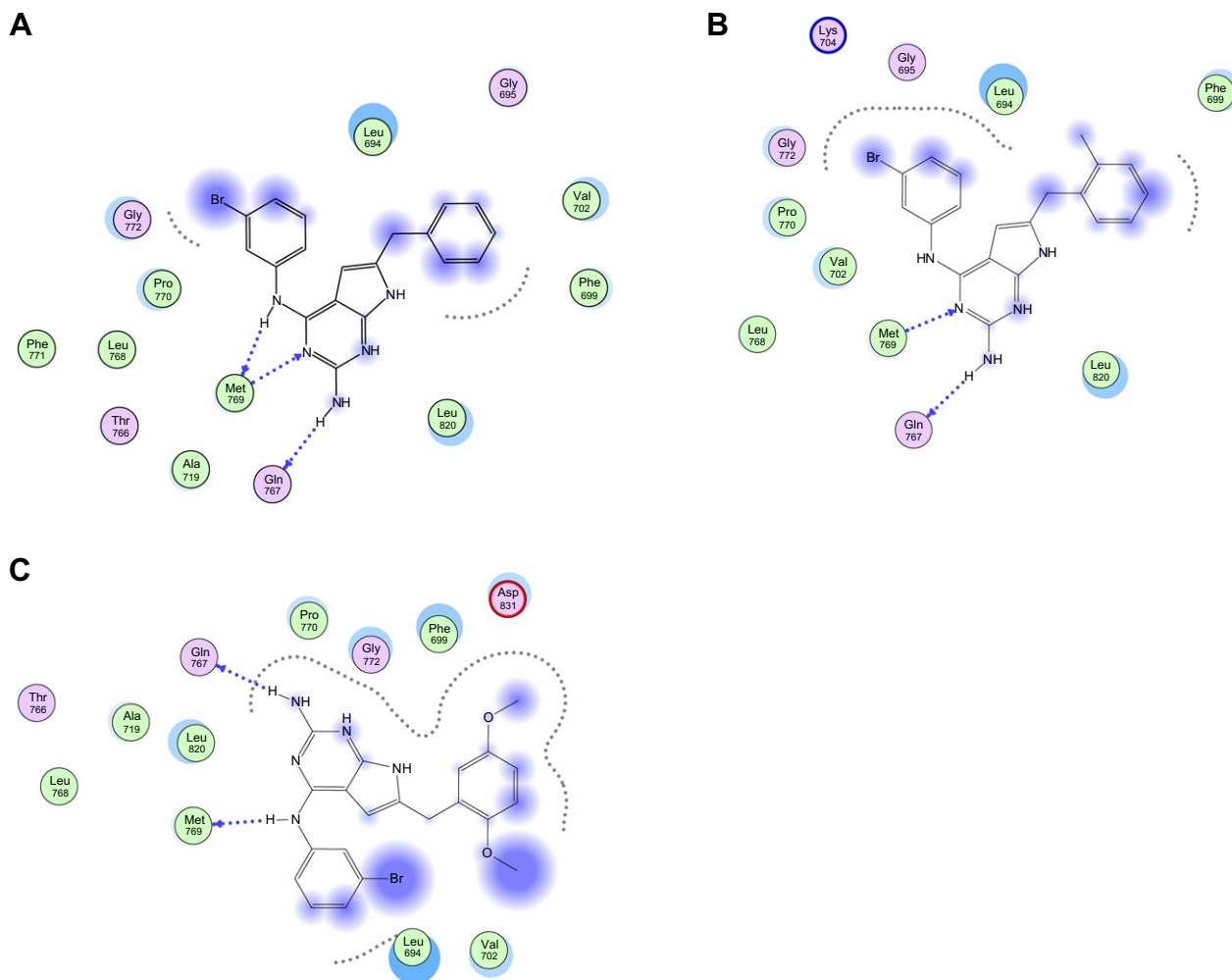


Figure 7. Ligand interaction plots of docked poses of **1** (A), **2** (B), and **3** (C) in the EGFR active site.

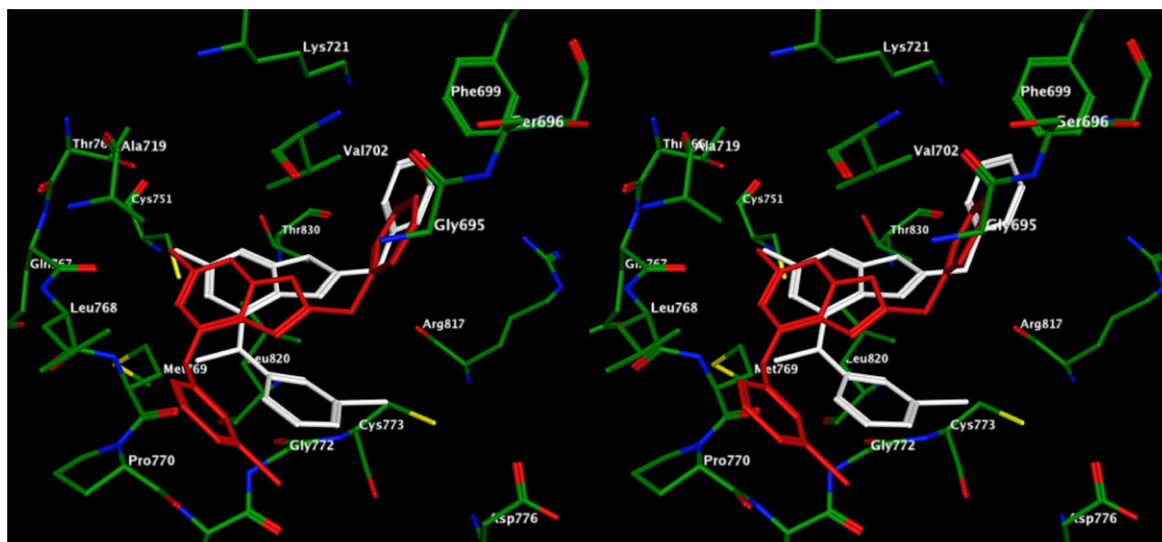


Figure 8. Stereoview. Overlay of docked poses of **1** (red) and **4** (white) in EGFR active site.

compound adopts a binding mode different from that seen with the docked poses of **1–3**. In the docked pose of **12** (Fig. 10), the 2-NH₂ moiety is involved in the lone Hinge region hydrogen bond. The 4-N and N7-methyl groups alter the conformation of the mol-

ecule and permits the anilino portion to access Hydrophobic site I. The 2',5'-dimethoxybenzyl side chain accesses the Sugar binding pocket and is placed in a hydrophobic site formed by Leu694, Phe699, and Val702. The 2',5'-dimethoxy moieties provides

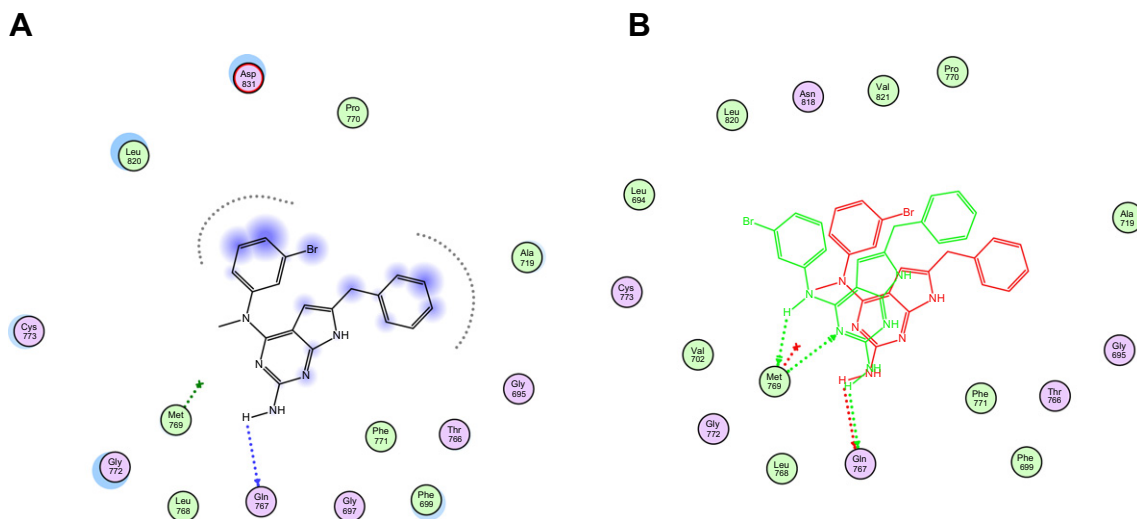


Figure 9. (A) Ligand interaction plots of docked pose of **4** in the EGFR active site. (B) Overlay of ligand interaction plots of docked poses of **4** (red) and **1** (green) in the EGFR active site. MOE 2009.10.

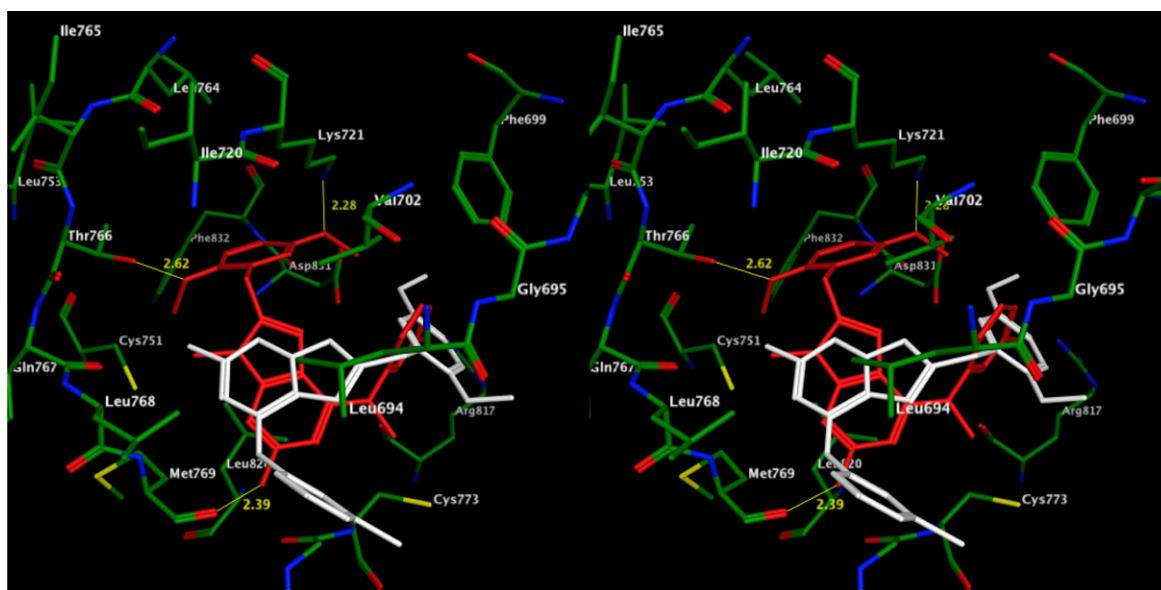


Figure 10. Stereoview. Overlay of docked poses of **12** (red) and **3** (white) in EGFR active site.

additional hydrogen bonds with Thr766 and Lys721. The conformational change due to 4-N, N7-dimethylation and additional interactions due to the nature and orientation of the benzyl side chain could be anticipated to compensate for the loss of hydrogen bonding by either the 4-N or N7 nitrogen atom and contribute to the increased potency of **12** against EGFR in whole cell assays compared with **3**.

All the mono- and di-methylated derivatives were comparatively inactive against VEGFR-2 in whole cell assays. This suggests that for VEGFR-2 inhibition, in whole cells, both the 4-NH and 7-NH protons are important for binding and necessary for activity. Whether this reflects space requirements or hydrogen bond donor ability at the 4-NH- and N7-positions is not clear and is currently under investigation.

In the PDGFR- β whole cell assay, compound **10**, the 4-N-methyl analogue, was the most potent and was about ninefold more potent than sunitinib, about threefold more potent than the standard, **20** and sevenfold more potent than its lead ana-

logue **3**. Compound **5**, which has a methyl group on the N7-position showed fourfold greater activity than sunitinib, comparable whole cell PDGFR- β inhibition with the standard, **20** and was over 20-fold more potent than the lead analogue **1**. The 4-N-methylated compound **7** showed increased activity compared with its lead **2**. This suggests that methylation on either the 4-NH or N7 increases the inhibitory activity against whole cell PDGFR- β . However, the N7-methylation of **1** to afford **5** increases the activity against whole cell PDGFR- β almost three-times greater than that for **10** over **3**.

There is currently no crystal structure of PDGFR- β bound to a ligand. Using the structure of c-KIT kinase complex (PDB: 1PKG, chain A)²³ as the template a homology model of PDGFR- β was generated using the Molecular Operating Environment (MOE 2007.09) suite.²⁴ Molecular modeling studies were performed using Flexx 3.1.2 as described above in an attempt to explain the increased activity of **10** compared with **3** against whole cell assays for PDGFR- β .

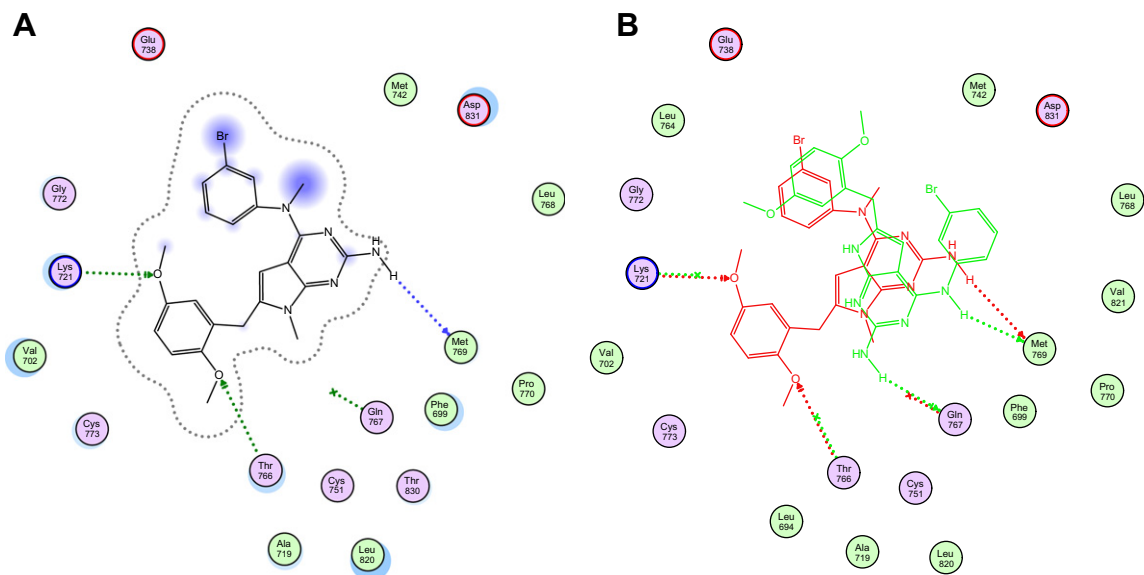


Figure 11. (A) Ligand interaction plots of docked pose of **12** in the EGFR active site. (B) Overlay of ligand interaction plots of docked poses of **12** (red) and **3** (green) in the EGFR active site.

Figure 12 shows the best docked pose of **3** within 2 kcal/mol of the lowest energy pose in the active site of the homology model of PDGFR- β . In this pose the pyrrolo[2,3-*d*]pyrimidine ring of **3** rests in the Adenine binding region and forms hydrogen bonds with Glu682 and Cys684 in the Hinge region via the N-1, 2-NH₂, and N-7 nitrogen atoms. These interactions serve to anchor the molecule and permit the anilino moiety to access Hydrophobic site I where it can interact with hydrophobic residues Ala848, Val614, and Leu606. The 2'-methoxy substituent on the 6-benzyl moiety can form a hydrogen bond with the backbone of Asp688. The docked pose of **10** in the homology model (Fig. 13) also maintains these interactions seen in the docked pose of **3**. In addition, **10**, which is methylated at the 4-N, binds in a mode which orients the anilino moiety deeper in Hydrophobic Site I. The bromo-

phenyl residues can form hydrophobic interactions with Val614, Leu606, Val665 (not shown), Phe845 and Ala848 and the side chain of Lys634. Additionally, the methyl group on the 4-N can form hydrophobic interactions with Val614 and Ala848 and provide additional stabilization of the pose. Together, these interactions could account, in part, for the improvement in activity of **10** over the lead compound **3**. Figure 14 shows the ligand interaction plots for **3** and **10** in the active site of the PDGFR- β homology model (see Fig. 14).

The docked pose of **5** (not shown) was similar to binding Mode II (Fig. 4). Hydrogen bonding interactions with the 2-NH₂ and 4-NH moieties were maintained with the Hinge region. The anilino moiety occupied Hydrophobic region II while the 6-benzyl moiety occupied the Sugar binding pocket.

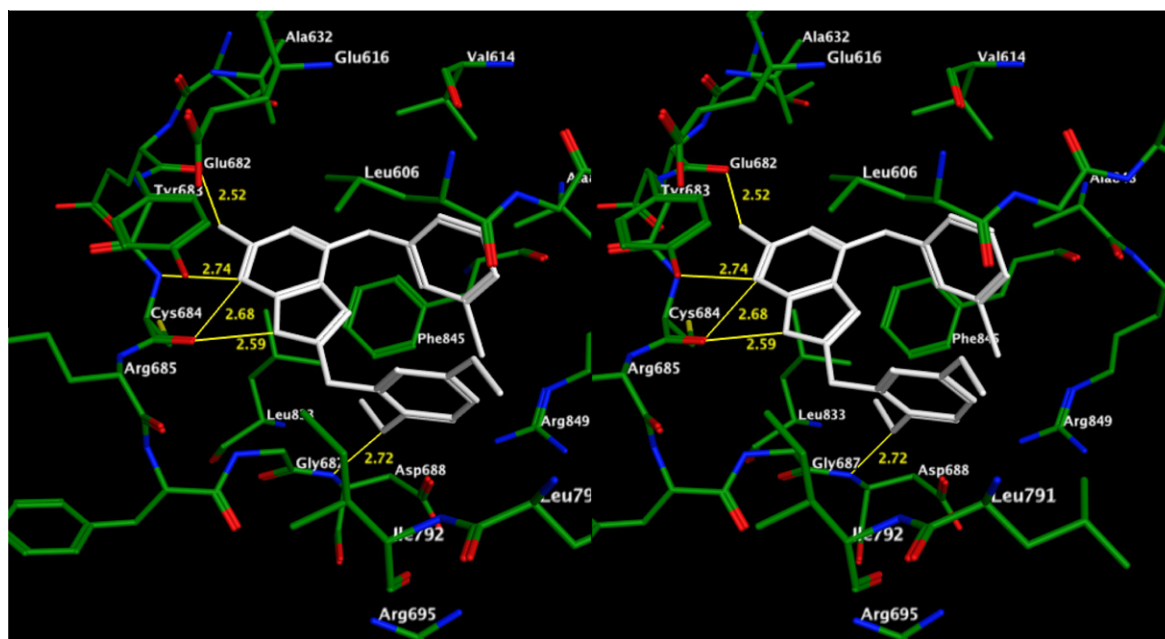


Figure 12. Stereoview. Docked pose of **3** (white) in PDGFR- β homology model.

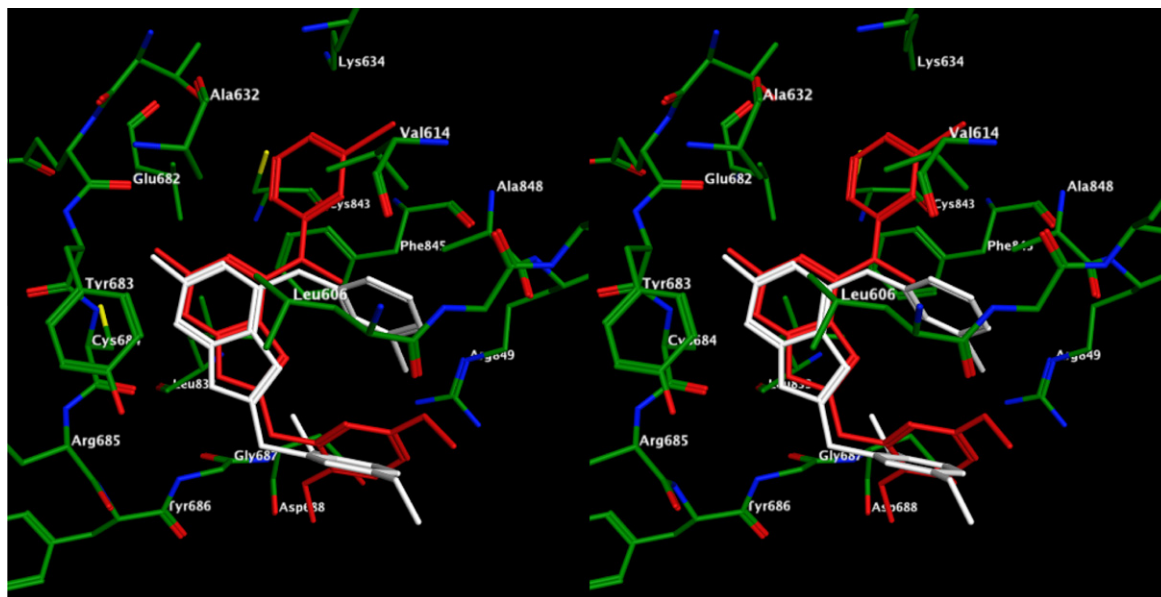


Figure 13. Stereoview. Overlay of docked poses of **10** (red) and **3** (white) in PDGFR- β homology model.

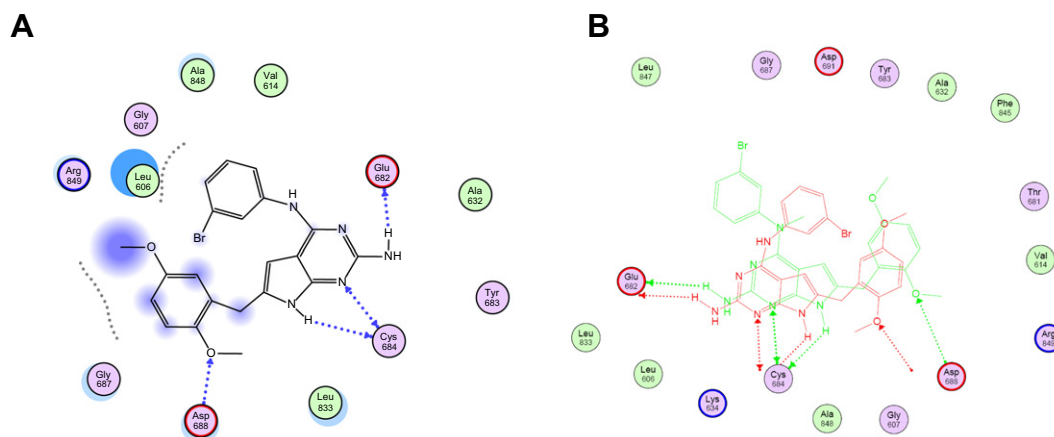


Figure 14. (A) Ligand interaction plots of docked pose of **3** in the PDGFR- β model. (B) Overlay of ligand interaction plots of docked poses of **3** (red) and **10** (green) in the PDGFR- β model.

Cytotoxicity studies against the growth of A431 (human cancer cells that over-express EGFR) in culture provided interesting results. All of the methylated compounds were less potent than the standard compound, cisplatin. The most potent compound was the N7-methyl substituted compound **5**. This was comparable with its lead **1**. However, compound **2** which was ninefold more potent than the standard, cisplatin against A431 when substituted at the 4-N or N7 or both, afforded compounds (**7–9**) that were inactive. The same modification for compound **3** also afforded inactive compounds (**10–11**). This suggests that 4-N- or N7-methylation is not conducive to A431 cytotoxicity. The data for most of the analogues do not correlate EGFR inhibitory activity (or inactivity) with A431 inhibitory activity (or inactivity). The most potent analogues against EGFR, compounds **9** and **12**, were inactive against A431 cells; compounds **5** and **11** which were completely inactive against EGFR showed the most potent inhibitory activity against A431 among all the methylated analogues. These unexpected results for A431 inhibition could reflect transport and/or other factors which influence the cytotoxic activity against the growth of cells in culture.

In summary, nine 2-amino-4-*m*-bromoanilino-6-benzyl pyrrolo[2,3-*d*]pyrimidines **4–12** were designed and synthesized as RTK inhibitors. The preliminary evaluation indicates that the compounds have high potency as antiangiogenic agents as indicated in the CAM assay. 4-N-Methylated compounds **7** and **10** showed the best activities and were better than the lead analogues. Compound **10** exhibited ninefold improved potency over sunitinib against PDGFR- β in the whole cell assay. Thus, mono- and di-methylation affords compounds with increased potency against EGFR and PDGFR- β compared to the corresponding desmethyl compounds. N-Methylation was detrimental to whole cell VEGFR-2 activity. Thus methylation at the 4-N or N7 position can be observed to influence inhibitory activity against the tested kinases. With the exception of **5**, the CAM assay indicates that all the other 4-N-methylated, N7-methylated and 4-N, N7-dimethylated analogues have good antiangiogenic activity comparable to the lead analogues **1–3** indicating that methylation at either or both positions do not hinder or enhance antiangiogenesis in the CAM assay. However, a clear cut SAR is not possible since these are whole cell assays and cell penetration and transport need to be considered

and because multiple growth factors, RTKs and endogenous anti-angiogenic molecules contribute to blood vessel growth in the CAM model. Since cell culture inhibitory studies afford the best models for translation to whole animal *in vivo* models we elected to use whole cell assays. Molecular modeling studies indicate the presence of multiple low energy binding modes for these molecules and explain, in part, the potent activities of **7**, **10**, and **12**. Thus, while general activity trends can be observed, it would be challenging to predict the preferred binding modes for these compounds in receptor tyrosine kinases. Compounds **7** and **10** are projected to start *in vivo* studies in the near future.

4. Experimental

Melting points were determined on a Mel-Temp II melting point apparatus with FLUKE 51 K/J electronic thermometer and are uncorrected. Nuclear magnetic resonance spectra for proton (^1H) were recorded on a Bruker WH-300 (300 MHz) spectrometer. The chemical shift values are expressed in ppm (parts per million) relative to tetramethylsilane as internal standard; s = singlet, d = doublet, t = triplet, q = quartet, m = multiplet, br s = broad singlet. The relative integrals of peak areas agreed with those expected for the assigned structures. Thin-layer chromatography (TLC) was performed on Polygram Sil G/UV254 silica gel plates with fluorescent indicator, and the spots were visualized under 254 and 365 nm illumination. Proportions of solvents used for TLC were by volume. Column chromatography was performed on 230–400 mesh silica gel purchased from Aldrich Chemical Co., Milwaukee, WI, USA. All evaporations were carried out *in vacuo* with a rotary evaporator. Analytical samples were dried *in vacuo* (0.2 mmHg) in an Abderhalden drying apparatus over P_2O_5 at 75–110 °C. Elemental analysis was performed by Atlantic Microlabs, Norcross, GA, USA. Element compositions are within $\pm 0.4\%$ of calculated values. Fractional moles of water or organic solvents frequently found in some analytical samples could not be prevented despite 24–48 h of drying *in vacuo* and were confirmed where possible by their presence in the ^1H NMR spectra. All solvents and chemicals were purchased from Aldrich Chemical Co. and Fisher Scientific and were used as received.

4.1. General procedure for the synthesis of compounds **15a–c**

In a 100 mL flask was placed 50% aqueous KOH solution (12 mL) and ether (40 mL). The mixture was cooled to 0–5 °C and nitrosomethylurea (5.9 g, 40 mmol) was added in part, stirring and the temperature maintained below 5 °C, the yellow solution was separated from water and dried with pellets of KOH. The ethereal diazomethane solution was used immediately for next step.

A solution of substituted phenyl acetic acid **13a–c** (5 mmol) in dry benzene (5 mL) and thionyl chloride (5 mL) was heated at reflux for 1 h and the solution was evaporated *in vacuo*. The resulting acid chloride was dissolved in ether (8 mL) and added dropwise with stirring to ethereal diazomethane at 0–5 °C. The yellow solution was allowed to stand at room temperature for 1 h, then hydrobromic acid (5 mL) was added dropwise to the solution and the yellow mixture was heated at 70–80 °C (oil bath) for 1 h. The reaction mixture was cooled to room temperature and the ether layer was separated, washed with water (10 mL), saturated NaHCO_3 aqueous solution (10 mL) and water (10 mL) and dried (anhydrous Na_2SO_4). The solution was evaporated to afford the α -bromomethyl substituted benzyl ketones **14a–c**. The compounds were not purified further and were used directly for the next step.

The α -bromomethyl substituted benzyl ketones **14a–c** were placed in a 50-mL flask and an equivalent amount of 2,6-diamino-

pyrimidin-4-one and DMF (15 mL) were added. The mixture was stirred at room temperature for 72 h. To the reaction mixture was added silica gel (3 g) and the solvent was evaporated to afford a plug. The silica gel plug obtained was loaded onto a silica gel column and eluted with $\text{CHCl}_3/\text{MeOH}$ (a gradient elution, 2% MeOH in CHCl_3 , and 5% MeOH in CHCl_3). Fractions containing the product (TLC) were pooled, and the solvent evaporated to afford pure 2-amino-4-oxo-6-substituted benzyl-pyrrolo[2,3-*d*]pyrimidines **15a–c**.

4.1.1. 2-Amino-4-oxo-6-benzyl-pyrrolo[2,3-*d*]pyrimidine (**15a**)

Compound **15a** was synthesized from **13a** (1.5 g, 8.9 mmol) using the general procedure described above and was obtained as a gray white solid (0.78 g, 37% for two steps): R_f 0.5 ($\text{CHCl}_3/\text{CH}_3\text{OH}$, 5:1); mp 270 °C; ^1H NMR ($\text{DMSO-}d_6$) δ 3.91 (s, 2H, CH_2), 5.84 (s, 1H, C5-CH), 6.0 (br s, 2H, NH_2 , exch), 7.10–7.30 (m, 5H, Ar-H), 11.10 (br s, 1H, NH, exch), 11.78 (s, 1H, NH, exch).

4.1.2. 2-Amino-4-oxo-6-(2-methylbenzyl)-pyrrolo[2,3-*d*]pyrimidine (**15b**)

Compound **15b** was synthesized from **13b** (3.0 g, 20 mmol) using the general procedure described above and was obtained as a light red solid (1.02 g, 20% for two steps): R_f 0.52 ($\text{CHCl}_3/\text{CH}_3\text{OH}$, 5:1); mp 290 °C; ^1H NMR ($\text{DMSO-}d_6$) δ 2.22 (s, 3H, CH_3), 3.79 (s, 2H, CH_2), 5.68 (s, 1H, C5-CH), 5.99 (br s, 2H, NH_2 , exch), 7.15–7.30 (m, 4H, Ar-H), 10.15 (br s, 1H, NH, exch), 10.92 (s, 1H, NH, exch).

4.1.3. 2-Amino-4-oxo-6-(2,5-dimethoxybenzyl)-pyrrolo[2,3-*d*]pyrimidine (**15c**)

Compound **15c** was synthesized from **13c** (3.92 g, 20 mmol) using the general procedure described above and was obtained as a light yellow solid (1.42 g, 24% for two steps): R_f 0.61 ($\text{CHCl}_3/\text{CH}_3\text{OH}$, 5:1); mp 275 °C; ^1H NMR ($\text{DMSO-}d_6$) δ 3.65 (s, 3H, CH_3), 3.73 (s, 3H, CH_3), 5.77 (s, 1H, C5-CH), 5.99 (br s, 2H, NH_2 , exch), 6.67–6.89 (m, 3H, Ar-H), 10.15 (br s, 1H, NH, exch), 11.0 (br s, 1H, NH, exch).

4.2. General procedure for the synthesis of compounds **16a–c**

The appropriate compound **15a–c** and trimethylacetic anhydride was heated at reflux for 3 h. The cooled solution was poured into a large quantity of hexane and the precipitate obtained was filtered and dried over P_2O_5 . The compounds obtained were used for the next reaction without further purification.

4.2.1. 2-Pivaloylamino-4-oxo-6-benzyl-pyrrolo[2,3-*d*]pyrimidine (**16a**)

Compound **16a** was synthesized from **15a** (0.33 g, 1.37 mmol) using the general procedure described above and was obtained as a light brown solid (0.32 g, 71%): R_f 0.50 ($\text{CHCl}_3/\text{CH}_3\text{OH}$, 10:1); mp 230 °C; ^1H NMR ($\text{DMSO-}d_6$) δ 1.23 (s, 9H, $\text{C}(\text{CH}_3)_3$), 3.95 (s, 2H, CH_2), 6.05 (s, 1H, C5-CH), 7.23–7.30 (m, 5H, Ar-H), 10.75 (br s, 1H, NH, exch), 11.60 (br s, 1H, NH, exch), 11.88 (br s, 1H, NH, exch).

4.2.2. 2-Pivaloylamino-4-oxo-6-(2-methylbenzyl)-pyrrolo[2,3-*d*]pyrimidine (**16b**)

Compound **16b** was synthesized from **15b** (0.58 g, 2.28 mmol) using the general procedure described above and was obtained as a light red solid (0.52 g, 67%): R_f 0.65 ($\text{CHCl}_3/\text{CH}_3\text{OH}$, 5:1); mp 260 °C; ^1H NMR ($\text{DMSO-}d_6$) δ 1.24 (s, 9H, $\text{C}(\text{CH}_3)_3$), 2.27 (s, 3H, CH_3), 3.93 (s, 2H, CH_2), 5.88 (s, 1H, C5-CH), 7.07–7.17 (m, 4H, Ar-H), 10.76 (br s, 1H, NH, exch), 11.51 (br s, 1H, NH, exch), 11.81 (br s, 1H, NH, exch).

4.2.3. 2-Pivaloylamino-4-oxo-6-(2,5-dimethoxybenzyl)-pyrrolo[2,3-d]pyrimidine (16c)

Compound **16c** was synthesized from **15c** (0.53 g, 1.38 mmol) using the general procedure described above and was obtained as a light yellow solid (0.55 g, 81%): R_f 0.45 (CHCl₃/CH₃OH, 10:1); mp 250 °C; ¹H NMR (DMSO-*d*₆); δ 1.20 (s, 9H, C(CH₃)₃), 3.65 (s, 3H, OCH₃), 3.74 (s, 3H, OCH₃), 3.86 (s, 2H, CH₂), 5.96 (s, 1H, C5-CH), 6.60–6.93 (m, 3H, Ar-H), 10.75 (br s, 1H, NH, exch), 11.53 (br s, 1H, NH, exch), 11.87 (br s, 1H, NH, exch).

4.3. General procedure for the synthesis of 17a–c

In a 50 mL round-bottom flask was placed **16a–c** and POCl₃ (5 mL). The mixture was heated to reflux for 2 h. After evaporation of the excess of POCl₃, ice-cold water was added. The reaction mixture was neutralized with NH₃·H₂O, and extracted with CHCl₃ (3×50 mL). The organic phase was combined and dried with Na₂SO₄. Concentration of the chloroform afforded a brown solid that was dissolved in chloroform (2–3 mL) again and was placed to the top of a 15 × 150 mm chromatographic column and eluted with 0.1% methanol in chloroform. Fractions containing the product were pooled and evaporated to afford pure compounds **17a–c**.

4.3.1. 2-Pivaloylamino-4-chloro-6-benzyl-pyrrolo[2,3-d] pyrimidine (17a)

Compound **17a** was synthesized from **16a** (0.30 g, 0.92 mmol) using the general procedure described above and was obtained as a yellow solid (0.10 g, 31%): R_f 0.50 (CHCl₃/CH₃OH, 10:1); mp 131.3–133.1 °C; ¹H NMR (DMSO-*d*₆) δ 1.20 (s, 9H, C(CH₃)₃), 4.07 (s, 2H, CH₂), 6.17 (s, 1H, C5-CH), 7.23–7.31 (m, 5H, Ar-H), 9.96 (br s, 1H, NH, exch), 12.36 (br s, 1H, NH, exch).

4.3.2. 2-Pivaloylamino-4-chloro-6-(2-methylbenzyl)-pyrrolo[2,3-d]pyrimidine (17b)

Compound **17b** was synthesized from **16b** (0.50 g, 1.48 mmol) using the general procedure described above and was obtained as a yellow solid (0.20 g, 38%): R_f 0.65 (CHCl₃/CH₃OH, 10:1); mp 80–82 °C; ¹H NMR (DMSO-*d*₆) δ 1.22 (s, 9H, C(CH₃)₃), 2.37 (s, 3H, CH₃), 4.06 (s, 2H, CH₂), 5.98 (s, 1H, C5-CH), 7.17–7.19 (m, 4H, Ar-H), 10.00 (br s, 1H, NH, exch), 12.37 (br s, 1H, NH, exch).

4.3.3. 2-Pivaloylamino-4-chloro-6-(2,5-dimethoxybenzyl)-pyrrolo[2,3-d]pyrimidine (17c)

Compound **17c** was synthesized from **16c** (0.55 g, 1.43 mmol) using the general procedure described above and was obtained as a yellow solid (0.45 g, 78%): R_f 0.69 (CHCl₃/CH₃OH, 10:1); mp 129.0–131.5 °C; ¹H NMR (DMSO-*d*₆) δ 1.25 (s, 9H, C(CH₃)₃), 3.83 (s, 3H, OCH₃), 3.98 (s, 3H, OCH₃), 4.12 (s, 2H, CH₂), 6.02 (s, 1H, C5-CH), 6.78–6.94 (m, 3H, Ar-H), 9.96 (br s, 1H, NH, exch), 12.28 (br s, 1H, NH, exch).

4.4. General procedure for the synthesis of compounds 4, 7, and 10

Compounds **17a–c** and 3-bromo-*N*-methyl aniline (1.5 equiv), *i*-PrOH (10 mL), and 2–3 drops of conc HCl were placed in a 50-mL flask. The mixture was heated to reflux overnight. After evaporation of the solvent, the residue was dissolved in 1,4-dioxane (10 mL), and 15% KOH aqueous solution (2 mL) was added. The reaction mixture was heated to reflux for 10 h. The solvent was removed under reduced pressure to give syrup. Water (20 mL) was added and the solution was extracted with chloroform (3×50 mL). The organic phase was combined and dried over anhydrous Na₂SO₄. Evaporation of the chloroform afforded a solid that was dissolved in methanol, and then 250 mg silica gel was added and the solvent removed in vacuo to afford a dry plug. This plug was placed on the top of a 15 × 150 mm column and eluted with

chloroform. Fractions containing the product (tlc) were pooled and evaporated to afford pure **4**, **7**, and **10**.

4.4.1. 2-Amino-4-(*N*-methyl-*m*-bromoanilino)-6-benzyl-pyrrolo[2,3-d]pyrimidine (4)

Compound **4** was synthesized from **17a** (0.20 g, 0.58 mmol) using the general procedure described above and was obtained as a light yellow solid (33 mg, 14%): R_f 0.33 (CHCl₃/CH₃OH, 10:1); mp 179.5–180.7 °C; ¹H NMR (DMSO-*d*₆) δ 3.42 (s, 3H, NCH₃), 3.68 (s, 2H, CH₂), 4.34 (s, 1H, CH), 5.63 (br s, 2H, NH₂, exch), 7.1–7.4 (m, 5H, Ar-H), 10.77 (br s, 1H, NH, exch). Anal. (C₂₀H₁₈BrN₅): C, H, N, Br.

4.4.2. 2-Amino-4-(*N*-methyl-*m*-bromoanilino)-6-(2-methylbenzyl)-pyrrolo[2,3-d]pyrimidine (7)

Compound **7** was synthesized from **17b** (0.20 g, 0.58 mmol) using the general procedure described above and was obtained as a white-off solid (25 mg, 14%): R_f 0.51 (CHCl₃/CH₃OH, 10:1); mp 176.6–177.9 °C; ¹H NMR (DMSO-*d*₆) δ 2.27 (s, 3H, CH₃-Ph), 3.66 (s, 3H, NCH₃), 4.12 (s, 2H, CH₂), 5.72 (br s, 2H, NH₂, exch), 6.99 (s, 1H, C5-CH), 7.07–7.41 (m, 7H, Ar-H), 10.79 (br s, 1H, NH, exch). Anal. (C₂₁H₂₀BrN₅): C, H, N, Br.

4.4.3. 2-Amino-4-(*N*-methyl-*m*-bromoanilino)-6-(2,5-dimethoxybenzyl)-pyrrolo[2,3-d]pyrimidine (10)

Compound **10** was synthesized from **17c** (0.15 g, 0.42 mmol) using the general procedure described above and was obtained as a white-off solid (35 mg, 20%): R_f 0.52 (CHCl₃/CH₃OH, 10:1); mp 212–214 °C; ¹H NMR (DMSO-*d*₆) δ 3.39 (s, 3H, NCH₃), 3.57 (s, 3H, OCH₃), 3.63 (s, 3H, OCH₃), 4.24 (s, 2H, CH₂), 5.62 (br s, 2H, NH₂, exch), 6.6 (s, 1H, C5-CH), 6.82–6.69 (m, 3H, Ar-H), 7.26–7.43 (m, 3H, Ar-H), 10.7 (br s, 1H, NH, exch). Anal. (C₂₂H₂₂BrN₅O₂·0.9CH₃OH): C, H, N, Br.

4.5. General procedure for the synthesis of 18a–c

Compounds **17a–c** were dissolved in THF (10 mL) and cooled down to 0 °C, 1.5 equiv NaH was added into the mixture and stirred for 10 min. adding the MeI dropwise to the reaction mixture and stirring for another 3 h. Water (10 mL) was added slowly to the reaction solution in an ice-bath, and the solution was extracted with ethyl acetate (3 × 50 mL). The organic phase was combined and dried with anhydrous Na₂SO₄. Concentration of the ethyl acetate afforded a solid that was dissolved in methanol, and then 250 mg silica gel was added and removed the solvent in vacuo to afford a dry plug. This plug was placed on the top of a 15 × 150 mm column and eluted with chloroform. Fractions containing the product were pooled and evaporated to afford **18a–c**.

4.5.1. 2-Pivaloylamino-4-chloro-6-benzyl-7-methyl-pyrrolo[2,3-d]pyrimidine (18a)

Compound **18a** was synthesized from **17a** (0.15 g, 0.42 mmol) using the general procedure described above and was obtained as a white-off solid (90 mg, 58%): R_f 0.84 (CHCl₃/CH₃OH, 10:1); mp 190.5–192.1 °C; ¹H NMR (DMSO-*d*₆) δ 1.21 (s, 9H, C(CH₃)₃), 3.60 (s, 3H, NCH₃), 4.22 (s, 2H, CH₂), 6.18 (s, 1H, C5-CH), 7.28–7.35 (m, 5H, Ar-H), 10.04 (br s, 1H, NH, exch).

4.5.2. 2-Pivaloylamino-4-chloro-6-(2-methylbenzyl)-7-methyl-pyrrolo[2,3-d]pyrimidine (18b)

Compound **18b** was synthesized from **17b** (0.35 g, 0.98 mmol) using the general procedure described above and was obtained as a yellow solid (0.2 g, 56%): R_f 0.86 (CHCl₃/CH₃OH, 10:1); mp 180.9–182.2 °C; ¹H NMR (DMSO-*d*₆) δ 1.23 (s, 9H, C(CH₃)₃), 2.37 (s, 3H, CH₃), 3.67 (s, 3H, NCH₃), 4.16 (s, 2H, CH₂), 5.98 (s, 1H, C5-CH), 7.17–7.19 (m, 4H, Ar-H), 10.09 (br s, 1H, NH, exch).

4.5.3. 2-Pivaloylamino-4-chloro-6-(2,5-dimethoxybenzyl)-7-methyl-pyrrolo[2,3-*d*]pyrimidine (**18c**)

Compound **18c** was synthesized from **17c** (0.45 g, 1.11 mmol) using the general procedure described above and was obtained as a yellow solid (0.36 g, 77%): R_f 0.84 (CHCl₃/CH₃OH, 10:1); mp 77.3–78.7 °C; ¹H NMR (DMSO-*d*₆) δ 1.23 (s, 9H, C(CH₃)₃), 3.26 (s, 3H, NCH₃), 3.66 (s, 3H, OCH₃), 3.85 (s, 3H, OCH₃), 4.18 (s, 2H, CH₂), 6.12 (s, 1H, C5-CH), 6.63–7.0 (m, 3H, Ar-H), 10.13 (br s, 1H, NH, exch).

4.6. General procedure for the synthesis of **5**, **8**, and **11**

Compounds **18a–c** and 3-bromo-aniline (1.5 equiv), *i*-PrOH (10 mL), and 2–3 drops of conc. HCl were placed in a 50-mL flask. The mixture was heated to reflux for 45 m. After evaporation of the solvent, the residue was dissolved in 1,4-dioxane (10 mL), and 15% KOH aqueous solution (2 mL) was added. The reaction mixture was heated to reflux for 10 h. The solvent was removed under reduced pressure to give syrup, and then water (20 mL) was added and the solution was extracted with chloroform (3 × 50 mL). The organic phase was combined and dried with anhydrous Na₂SO₄. Concentration of the chloroform afforded a residue that was dissolved in methanol, and then 250 mg silica gel was added and removed the solvent in vacuo to afford a dry plug. This plug was placed on the top of a 15 × 150 mm column and eluted with 2% methanol in chloroform. Fractions containing the product were pooled and evaporated to afford pure **5**, **8**, and **11**.

4.6.1. 2-Amino-4-(*m*-bromoanilino)-6-benzyl-7-methyl-pyrrolo[2,3-*d*]pyrimidine (**5**)

Compound **5** was synthesized from **18a** (0.10 g, 0.28 mmol) using the general procedure described above and was obtained as a yellow solid (63 mg, 55%): R_f 0.53 (CHCl₃/CH₃OH, 10:1); mp 155.7–157.6 °C; ¹H NMR (DMSO-*d*₆) δ 3.66 (s, 3H, NCH₃), 4.03 (s, 2H, CH₂), 5.89 (br s, 2H, NH₂, exch), 6.18 (s, 1H, C5-CH), 7.06–7.35 (m, 5H, Ar-H), 8.01–8.11 (m, 2H, Ar-H), 8.98 (br s, 1H, NH, exch). Anal. (C₂₀H₁₈BrN₅): C, H, N, Br.

4.6.2. 2-Amino-4-(*m*-bromoanilino)-6-(2-methylbenzyl)-7-methyl-pyrrolo[2,3-*d*]pyrimidine (**8**)

Compound **8** was synthesized from **18b** (0.13 g, 0.35 mmol) using the general procedure described above and was obtained as a yellow solid (86 mg, 58%): R_f 0.26 (CHCl₃/CH₃OH, 20:1); mp 173.5–174.1 °C; ¹H NMR (DMSO-*d*₆) δ 2.36 (s, 3H, CH₃-Ph), 3.6 (s, 3H, CH₃N), 3.9 (s, 2H, CH₂), 5.92 (br s, 2H, NH₂, exch), 5.98 (s, 1H, CH), 7.06–7.21 (m, 4H, Ph-H), 8.01–8.08 (m, 3H, Ph-H), 9.0 (br s, 1H, NH, exch). Anal. (C₂₁H₂₀BrN₅): C, H, N, Br.

4.6.3. 2-Amino-4-(*m*-bromoanilino)-6-(2,5-dimethoxybenzyl)-7-methyl-pyrrolo[2,3-*d*]pyrimidine (**11**)

Compound **11** was synthesized from **18c** (0.20 g, 0.48 mmol) using the general procedure described above and was obtained as a yellow solid (95 mg, 42%): R_f 0.41 (CHCl₃/CH₃OH, 5:1); mp 78–80 °C; ¹H NMR (DMSO-*d*₆) δ 3.45 (s, 3H, NCH₃), 3.69 (s, 3H, OCH₃), 3.73 (s, 3H, OCH₃), 3.91 (s, 2H, CH₂), 5.84 (br s, 2H, NH₂, exch), 6.09 (s, 1H, C5-CH), 6.66–7.18 (m, 5H, Ar-H), 8.00–8.10 (m, 2H, Ar-H), 8.93 (br s, 1H, NH, exch). Anal. (C₂₂H₂₂BrN₅O₂·0.6-CH₃OH): C, H, N, Br.

4.7. General procedure for the synthesis of **6**, **9**, and **12**

Compound **18a–c**, 3-bromo-*N*-methyl aniline (1.5 equiv), *i*-PrOH (10 mL), and 2–3 drops of conc. HCl were placed in a 50-mL flask. The mixture was heated to reflux for 45 m. After evaporation of the solvent, the residue was dissolved in 1,4-dioxane (10 mL), and 15% KOH aqueous solution (2 mL) was added. The reaction mix-

ture was heated to reflux for 10 h. The solvent was removed under reduced pressure, and then water (20 mL) was added and the resulted solution was extracted with chloroform (3 × 50 mL). The organic phase was combined and dried with anhydrous Na₂SO₄. Concentration of the chloroform afforded a solid that was dissolved in methanol, and then 250 mg silica gel was added and removed the solvent in vacuo to afford a dry plug. This plug was placed on the top of a 15 × 150 mm column and eluted with 2% methanol in chloroform. Fractions containing the product were pooled and evaporated to afford pure **6**, **8**, and **12**.

4.7.1. 2-Amino-4-(*N*-methyl-*m*-bromoanilino)-6-benzyl-7-methyl-pyrrolo[2,3-*d*]pyrimidine (**6**)

Compound **6** was synthesized from **18a** (0.17 g, 0.48 mmol) using the general procedure described above and was obtained as a yellow solid (55 mg, 27%): R_f 0.52 (CHCl₃/CH₃OH, 10:1); mp 187.1–190.4 °C; ¹H NMR (DMSO-*d*₆) δ 3.42 (s, 3H, NCH₃), 3.80 (s, 3H, NCH₃), 4.30 (s, 2H, CH₂), 5.79 (br s, 2H, NH₂, exch), 6.99 (s, 1H, CH), 7.04–7.42 (m, 8H, Ar-H). Anal. (C₂₁H₂₀BrN₅·0.2H₂O): C, H, N, Br.

4.7.2. 2-Amino-4-(*N*-methyl-*m*-bromoanilino)-6-(2-methylbenzyl)-7-methyl-pyrrolo[2,3-*d*]pyrimidine (**9**)

Compound **9** was synthesized from **18b** (0.20 g, 0.54 mmol) using the general procedure described above and was obtained as a white-off solid (78 mg, 33%): R_f 0.40 (CHCl₃/CH₃OH, 10:1); mp 184–186.5 °C; ¹H NMR (DMSO-*d*₆) δ 2.15 (s, 3H, CH₃), 3.38 (s, 3H, NCH₃), 3.40 (s, 3H, NCH₃), 3.76 (s, 2H, CH₂), 4.08 (s, 1H, CH), 5.78 (br s, 2H, NH₂, exch), 6.82–7.38 (m, 8H, Ph-H). Anal. (C₂₂H₂₂BrN₅·0.2H₂O): C, H, N, Br.

4.7.3. 2-Amino-4-(*N*-methyl-*m*-bromoanilino)-6-(2,5-dimethoxybenzyl)-7-methyl-pyrrolo[2,3-*d*]pyrimidine (**12**)

Compound **12** was synthesized from **18c** (0.09 g, 0.22 mmol) using the general procedure described above and was obtained as a white-off solid (27 mg, 25%): R_f 0.53 (CHCl₃/CH₃OH, 10:1); mp 153.6–154.3 °C; ¹H NMR (DMSO-*d*₆) δ 3.48 (s, 3H, NCH₃), 3.63 (s, 3H, OCH₃), 3.67 (s, 3H, OCH₃), 4.2 (s, 2H, CH₂), 5.79 (br s, 2H, NH₂, exch), 6.41 (s, 1H, CH), 6.75–6.78 (m, 3H, Ph-H), 7.26–7.43 (m, 3H, Ph-H). Anal. (C₂₃H₂₄BrN₅O₂·0.7CH₃OH): C, H, N, Br.

5. Molecular modeling

Molecular modeling was performed using the X-ray crystal structure of erlotinib bound to EGFR (PDB ID: 1M17) using Flexx 3.1.2. The active site for docking was defined using amino acids within 6.5 Å cocrystallized ligand in the crystal structure. Polar hydrogen atoms of Thr766, Cys773, and Thr830 were permitted to rotate freely. Ligands for docking were prepared using the molecule builder in MOE 2009.10. Prior to docking, the ligands were imported into Flexx, atom types, protonation states and formal charges were assigned using default settings. Docking into the active site was performed using Triangle matching. The maximum number of solutions per iteration and the maximum number of solutions per fragment was set at 500. The top 10 poses were retained for each molecule from every docking run. The docked poses were exported and visualized using MOE 2009.10. Ligand interaction plots were calculated using MOE 2009.10.

Prior to docking of **1–12**, a docking run was performed using the native X-ray crystal structure ligand (erlotinib) as described above. The RMSD of the docked conformation of erlotinib was 0.9 Å compared to the crystal structure conformation of erlotinib. Flexx 3.1.2 was thus validated for our docking studies.

There is no known X-ray crystal structure of PDGFR- β . Thus, a homology model of PDGFR- β was created²⁵ and utilized for dock-

ing 1–12. Docking studies were performed using Flexx 3.1.2 using the same settings as described above. Docked poses were exported and visualized in MOE 2009.10. Ligand interaction plots were calculated using MOE 2009.10.

Acknowledgment

This work was supported, in part, by the National Institutes of Health and National Cancer Institute Grant CA98850 (A.G.).

Supplementary data

Supplementary data (results from elemental analysis. This material is available free of charge via the Internet) associated with this article can be found, in the online version, at [doi:10.1016/j.bmc.2010.05.049](https://doi.org/10.1016/j.bmc.2010.05.049).

References and notes

- Gangjee, A.; Zhao, Y.; Ihnat, M. A.; Green, D.; Miller, W. T. The 96th American Association for Cancer Research (AACR) Annual Meeting, Anaheim, CA, April 16–20, 2005, poster number 3946.
- Folkman, J. *Nat. Rev. Drug Disc.* **2007**, *6*, 273.
- Folkman, J. *Breast Cancer Res. Treat.* **1995**, *36*, 109.
- Bohle, A. S.; Kalthoff, H. *Langenbecks Arch. Surg.* **1999**, *38*, 4133.
- Hanahan, D.; Folkman, J. *Cell* **1996**, *1996*, 353.
- Ellis, L. M. *Hematol. Oncol. Clin. North Am.* **2004**, *18*, 1007. viii.
- Sun, L.; McMahon, G. *Drug Discovery Today* **2000**, *8*, 344.
- Dancey, J.; Sausville, E. A. *Nat. Rev. Drug Disc.* **2003**, *2*, 296.
- Bilodeau, M. T.; Fraley, M. E.; Hartman, G. D. *Expert Opin. Investig. Drugs* **2002**, *11*, 737.
- Bergsland, E. K. *Am. J. Health-Syst. Pharm.* **2004**, *61*, S12.
- Mandel, D. B.; Laird, A. D.; Xin, X.; Louie, S. G.; Christensen, J. G.; Li, G.; Schreck, R. E.; Abrams, T. J.; Ngai, T. J.; Lee, L. B.; Murray, L. J.; Carver, J.; Chan, E.; Moss, K. G.; Haznedar, J. O.; Sukbuntherrng, J.; Blake, R. A.; Sun, L.; Tang, C.; Miller, T.; Shirazian, S.; McMahon, G.; Cherrington, J. M. *Clin. Cancer Res.* **2003**, *9*, 327.
- Wilhelm, S. M.; Carter, C.; Tang, L.; Wilkie, D.; McNabola, A.; Rong, H.; Chen, C.; Zhang, X.; Vincent, P.; McHugh, M.; Cao, Y.; Shujath, J.; Gawlak, S.; Eveleigh, D.; Rowley, B.; Liu, L.; Adnane, L.; Lynch, M.; Auclair, D.; Taylor, I.; Gedrich, R.; Voznesensky, A.; Riedl, B.; Post, L. E.; Bollag, G.; Trail, P. A. *Cancer Res.* **2004**, *64*, 7099.
- Furet, P.; Caravatti, G.; Lydon, N.; Priestle, J.; Sowadski, J.; Trinks, U.; Traxler, P. *J. Comput. Aided Mol. Des.* **1995**, *9*, 465.
- Traxler, P.; Green, J.; Mett, H.; Sequin, U.; Furet, P. *J. Med. Chem.* **1999**, *42*, 1018.
- Gangjee, A.; Yang, J.; Ihnat, M.; Kamat, S. *Bioorg. Med. Chem.* **2003**, *11*, 5155.
- Gangjee, A.; Kurup, S.; Ihnat, M. A.; Green, D., unpublished results.
- Gangjee, A.; Namjoshi, O.; Yu, J.; Ihnat, M. A.; Thorpe, J. E.; Warnke, L. A. *Bioorg. Med. Chem.* **2008**, *16*, 5514.
- Stamos, J.; Sliwkowski, M. X.; Eigenbrot, C. *J. Biol. Chem.* **2002**, *277*, 46265.
- Flexx 3.1.2 BioSolveIT GmbH, An der Ziegelei 79, 53757 Sankt Augustin Germany. <http://www.biosolveit.de>.
- Constantine, K. L.; Mueller, L.; Metzler, W. J.; McDonnell, P. A.; Todderud, G.; Goldfarb, V.; Fan, Y.; Newitt, J. A.; Kiefer, S. E.; Gao, M.; Tortolani, D.; Vaccaro, W.; Tokarski, J. *J. Med. Chem.* **2008**, *51*, 6225.
- Boschelli, D. H. *Curr. Top. Med. Chem.* **2002**, *2*, 1051.
- Miki, A.; Miki, K.; Ueno, S.; Wersinger, D. M.; Berlinicke, C.; Shaw, G. C.; Usui, S.; Wang, Y.; Zack, D. J.; Campochiaro, P. A. *J. Cell. Physiol.* **2010**, *224*, 262.
- Mol, C. D.; Lim, K. B.; Sridhar, V.; Zou, H.; Chien, E. Y. T.; Sang, B.-C.; Nowakowski, J.; Kassel, D. B.; Cronin, C. N.; McRee, D. E. *J. Biol. Chem.* **2003**, *278*, 31461.
- MOE (Molecular Operating Environment). Distributor: Chemical Computing Group, 1010 Sherbrooke St. West, #910, Montreal, Canada H3A. <http://www.chemcomp.com>.
- Gangjee, A.; Zaware, N.; Raghavan, S.; Ihnat, M.; Shenoy, S.; Kisliuk, R. L. *J. Med. Chem.* **2010**, *53*, 1563.